Article:
Dong, Y., Chi, J., Ren, Z. et al. (7 more authors) (2023) Controlled Deformation of Soft Nanogel Particles Generates Artificial Biominerals with Ordered Internal Structure. Angewandte Chemie International Edition, 62 (19). e202300031. ISSN 1433-7851

https://doi.org/10.1002/anie.202300031

RESEARCH ARTICLE

Controlled Deformation of Soft Nanogel Particles Generates Artificial Biominerals with Ordered Internal Structure

Yingxiang Dong,[a,†] Jialin Chi,[b,e,†] Zelun Ren,[a] Biao Xiong,[a] Ziqing Liu,[a] Wenjun Zhang,*[,b] Lijun Wang,[b] Syuji Fujii,*[,c] Steven P. Armes,*[,d] and Yin Ning*[,a]

[a] Y Dong, Z Ren, B Xiong, Z Liu and Prof. Y Ning
College of Chemistry and Materials Science, Guangdong Provincial Key Laboratory of Functional Supramolecular Coordination Materials and Applications, Jinan University, Guangzhou 510632, China
E-mail: yinning@jnu.edu.cn

[b] Dr. J Chi, Prof. W Zhang and Prof. L Wang
College of Resources and Environment, Huazhong Agricultural University, Wuhan 430070, China
E-mail: wenjunzhang@hzau.edu.cn

[c] Prof. S Fujii
Department of Applied Chemistry, Faculty of Engineering, and Nanomaterials Microdevices Research Center, Osaka Institute of Technology, 5-16-1 Omiya, Asahi-ku, Osaka 535-8585, Japan
E-mail: syuji.fujii@oit.ac.jp

[d] Prof. S P Armes
Department of Chemistry, University of Sheffield, Brook Hill, Sheffield, South Yorkshire S3 7HF, UK
E-mail: s.p.armes@sheffield.ac.uk

[e] Dr J Chi
Present address: National-Regional Joint Engineering Research Center for Soil Pollution Control and Remediation in South China, Guangdong Key Laboratory of Integrated Agroenvironmental Pollution Control and Management, Institute of Eco-environmental and Soil Sciences, Guangdong Academy of Sciences, Guangzhou 510650, China

† These two authors contributed equally.

Supporting information for this article is given via a link at the end of the document.

Abstract: Biominerals can exhibit exceptional mechanical properties owing to their hierarchically-ordered organic/inorganic nanocomposite structure. However, synthetic routes to oriented artificial biominerals of comparable complexity remain a formidable technical challenge. Herein we design a series of soft, deformable nanogels that are employed as particulate additives to prepare nanogel@calcite nanocomposite crystals. Remarkably, such nanogels undergo a significant morphological change—from spherical to pseudo-hemispherical—depending on their degree of cross-linking. Such deformation occurs normal to the direction of growth of the (104) face of the calcite and the underlying occlusion mechanism is revealed by *in situ* atomic force microscopy studies. This model system provides new mechanistic insights regarding the formation of oriented structures during biomineralization and offers new avenues for the design of synthetic nanocomposites comprising aligned anisotropic nanoparticles.

Introduction

Various living organisms can generate biominerals with highly ordered/hierarchical structures by using biomacromolecules to control the nucleation and growth of inorganic crystals.[1] For example, mollusks grow tough shells in which aragonite layers are separated by an interlamellar organic matrix in a nacre-like structure.[2] Such organic/aragonite layers lie parallel to the surface of the shell, which confers excellent mechanical properties that are optimized for protection against predators. Mao and co-workers reported that artificial nacre can be prepared using an "assembly-and-mineralization" strategy.[3] More specifically, a laminated β-chitin matrix was used as a template to direct the mineralization of calcium carbonate, producing a synthetic nanocomposite material with comparable mechanical strength and fracture toughness to that of natural nacre. Despite the synthetic complexity, this is undoubtedly a remarkable achievement in biomimetic synthesis.

Recently, occlusion of diblock copolymer nanoparticles or polymer-stabilized inorganic nanoparticles within mineral host crystals has garnered considerable interest, not least because it offers an opportunity to investigate biomineralization.[4] Precise control over the surface chemistry and structure of such guest species enables identification of the critical parameters that dictate additive occlusion, thereby providing useful mechanistic insights.[5] Nevertheless, the rational synthesis of artificial biominerals possessing highly-oriented internal structure via nanoparticle occlusion has not been realized.

Various literature reports describe the construction of an oriented organic template prior to its mineralization.[3, 6] Alignment of such templates directs the formation of the final oriented structure. In the present study, we sought to exploit the intimate interaction between guest nanoparticles and host minerals to prepare a synthetic biomineral with an oriented internal structure without recourse to templates. We hypothesized that sufficiently soft isotropic nanoparticles should undergo *in situ* deformation during occlusion owing to local forces exerted by the growing crystal lattice. Moreover, this change in morphology may lead to oriented anisotropic nanoparticles within the host crystal. To test this hypothesis, we designed a series of tunably deformable spherical nanogels, which become hemispherical after their occlusion within calcite. Importantly, this change in morphology is oriented normal to the direction of growth of the (104) face of the inorganic calcite crystal. *In situ* atomic force microscopy (AFM) studies confirm that two types of deformation occur consecutively and provide new mechanistic insights regarding the formation

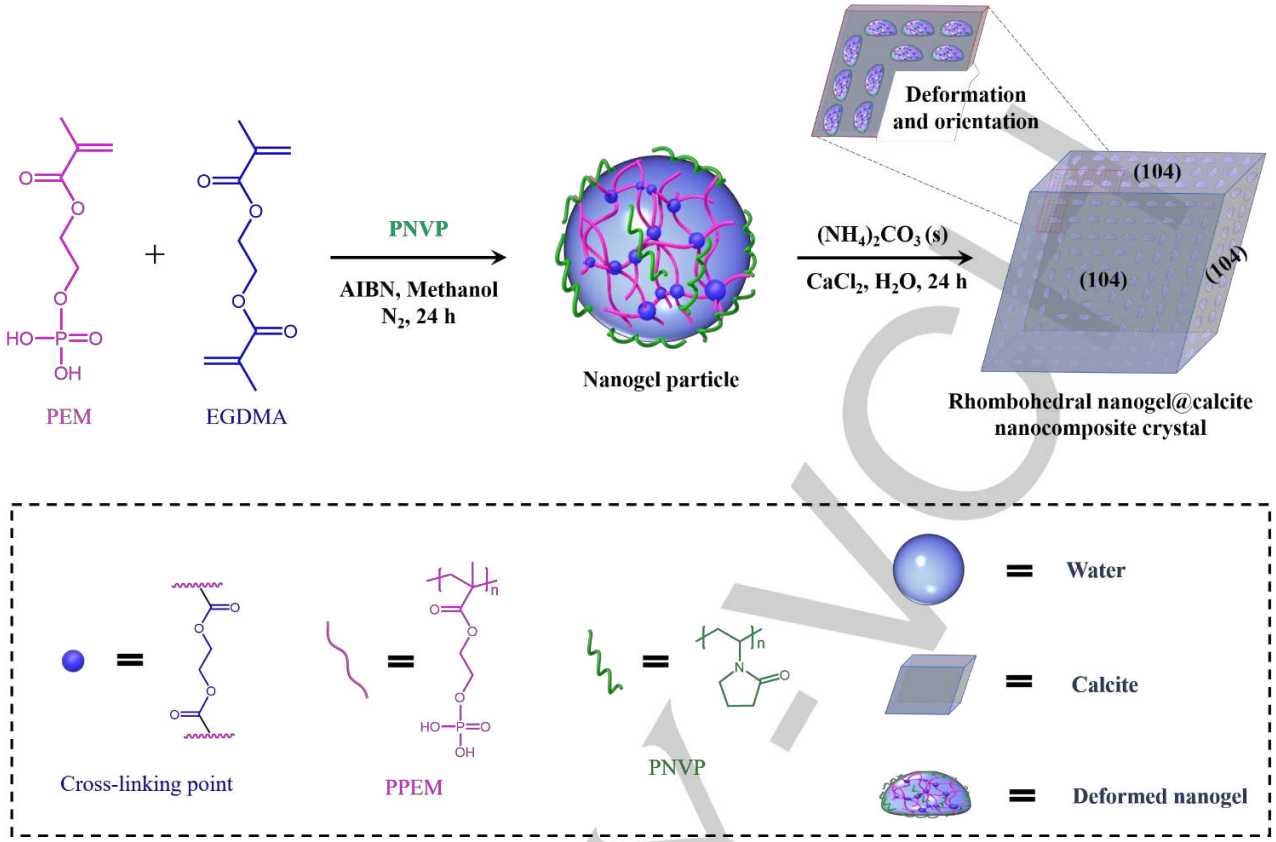

Scheme 1. Synthesis of nanogel particles via free radical dispersion copolymerization of PEM with various amounts of EGDMA cross-linker and their subsequent occlusion within calcite, leading to the formation of a nanogel@calcite nanocomposite in which deformed hemispherical nanogel particles are oriented along the {104} face of the rhombohedral host crystal. The dashed box defines each colored component featured in the schematic cartoon. N.B. The crystals and microgels shown in this Scheme are not drawn to scale.

of oriented nanostructures via biomineralization. Moreover, our approach offers a convenient synthetic route to a new class of organic-inorganic nanocomposites via nanoparticle occlusion.

Results and Discussion

Synthesis and characterization of nanogel particles. Nanogel particles were prepared via free radical dispersion copolymerization of 2-(phosphonooxy)ethyl methacrylate (PEM) with ethylene glycol dimethacrylate (EGDMA) in the presence of poly(*N*-vinylpyrrolidone) (PNVP) in methanol (see **Scheme 1**).[7] The PNVP plays a decisive role in the formation of nanogel particles. It not only serves as a precipitant that complexes with poly(2-(phosphonooxy)ethyl methacrylate) (PPEM) but also acts as a steric stabilizer to confer colloidal stability. The presence of EGDMA ensures cross-linking between the PPEM chains, resulting in the formation of water-swollen nanogel particles (**Scheme 1**).

Dynamic light scattering (DLS) studies indicated that such nanogels exhibited a unimodal particle size distribution (see **Figure S1**). Increasing the EGDMA content led to a higher degree of cross-linking and a reduction in the mean hydrodynamic diameter (**Figure S1**). Interestingly, the presence of 1.5 mM Ca^{2+} significantly reduced the hydrodynamic diameter. This suggests that such cations interact with the anionic PPEM network, causing nanogel shrinkage via additional ionic crosslinks.[8] Aqueous electrophoresis studies revealed that the zeta potential of such nanogels in the presence of 1.5 mM Ca^{2+} is significantly lower than that determined in the absence of Ca^{2+} (**Figure S2**), which indicates strong cation binding to the PPEM chains.[9] Moreover, scanning electron microscopy (SEM) and transmission electron microscopy (TEM) studies indicated that the nanogel particles are near-monodisperse (**Figure S3**). The number-average diameter of the dried nanogel particles estimated by electron microscopy is significantly smaller than the hydrodynamic z-average diameter reported by DLS. Although some difference would be expected owing to the effect of polydispersity, this relatively large difference indicates that such nanogels are highly swollen by water in aqueous media.[10]

Occlusion of nanogels within calcium carbonate ($CaCO_3$) crystals. $CaCO_3$ crystals (~40 μm) were precipitated in the presence of 1.5 mM $CaCl_2$ and 0.1% w/w nanogel particles in aqueous solution using the well-established ammonia diffusion method.[11] Perfect rhombohedral crystals with six smooth (104) faces were obtained in the absence of any nanogel (see **Figures 1a**). In contrast, crystals with rough surfaces and truncated edges were obtained in the presence of the nanogel particles (see insets in **Figures 1d, g, j**). Moreover, optical microscopy studies indicated that crystals precipitated in the presence of nanogel particles became opaque, suggesting successful occlusion of this additive (see **Figure S4**).[8a, 9] Raman spectroscopy studies (**Figure S5**) and powder X-ray diffraction analysis (PXRD, **Figure S6**)

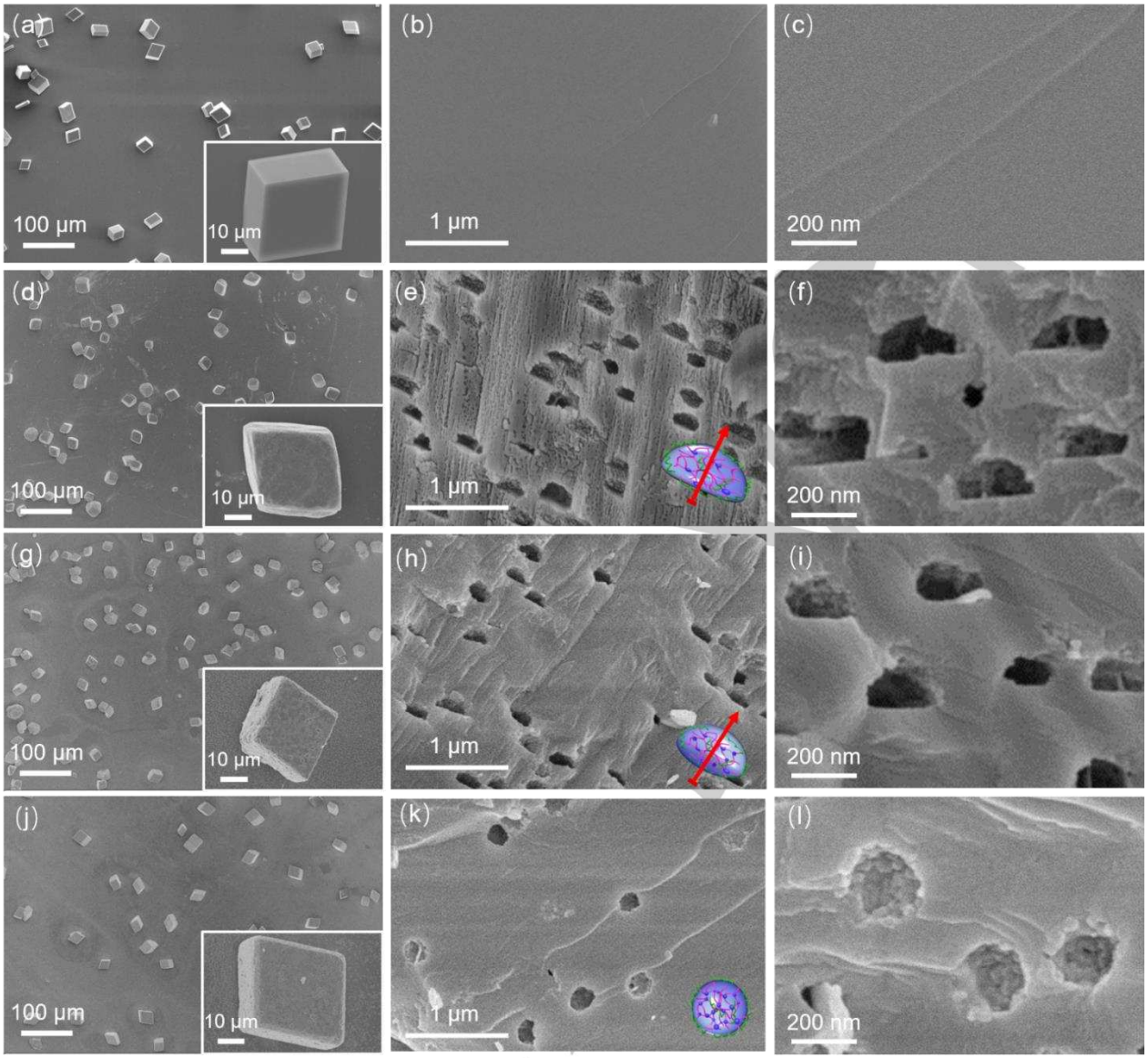

Figure 1. Occlusion of nanogel particles with varying EGDMA content within calcite crystals. Representative SEM images (a-c) obtained for calcite crystals mineralized in the absence of any additives and in the presence of 0.1% w/w nanogel particles with EGDMA contents of (d-f) 2.5%, (g-i) 5.0% and (j-l) 10.0%. The left-hand column shows the surface morphology of intact composite crystals while the central column presents cross-sectional images of randomly-fractured crystals. The right-hand column shows high magnification SEM images of the same randomly-fractured crystals, which reveal the morphology and roughness of the cavities. Insets within (a, d, g and j) depict high magnification images of individual crystals. Schematic cartoons within (e, h and k) indicate the morphology of the nanogel particles and the corresponding red arrows indicate the growth direction of the (104) face for rhombohedral calcite.

confirmed that the polymorph for all crystals was calcite, thus nanogel occlusion did not affect the crystal structure. SEM studies of the cross-sections of randomly-fractured crystals revealed the internal structure of these nanogel@calcite composite crystals (**Figure 1**). First, a featureless cross-section was observed for control calcite crystals (**Figures 1b-c**). In contrast, the cross-section of nanogel@calcite nanocomposite crystals contained many cavities, thus providing direct evidence for nanogel occlusion within the host lattice (**Figures 1e, h, k**). This is consistent with Fourier transform infrared (FTIR) spectra recorded for such crystals, which contained both an ester carbonyl stretching at 1725 cm^{-1} and an asymmetric stretching vibration for phosphate at 1158 cm^{-1}. These spectral features are characteristic of the nanogel particles (see **Figure S7**), which confirms their occlusion within the calcite crystals.

Second, the extent of occlusion within calcite was inversely related to the EGDMA content of the nanogel particles: correspondingly fewer cavities were observed on increasing the EGDMA content from 2.5% to 10.0% (see **Figure 1** and **Figure 2a**). This is because a higher degree of cross-linking restricts the nanogel deformability: this reduces the interaction between the anionic anchor groups and the growing calcite crystals, thus lowering the extent of occlusion. In this context, it is worth emphasizing that the non-ionic PNVP steric stabilizer chains do not promote nanogel occlusion: control experiments confirmed that PNVP-stabilized polystyrene nanoparticles could not be incorporated into calcite crystals (see **Figure S8**).

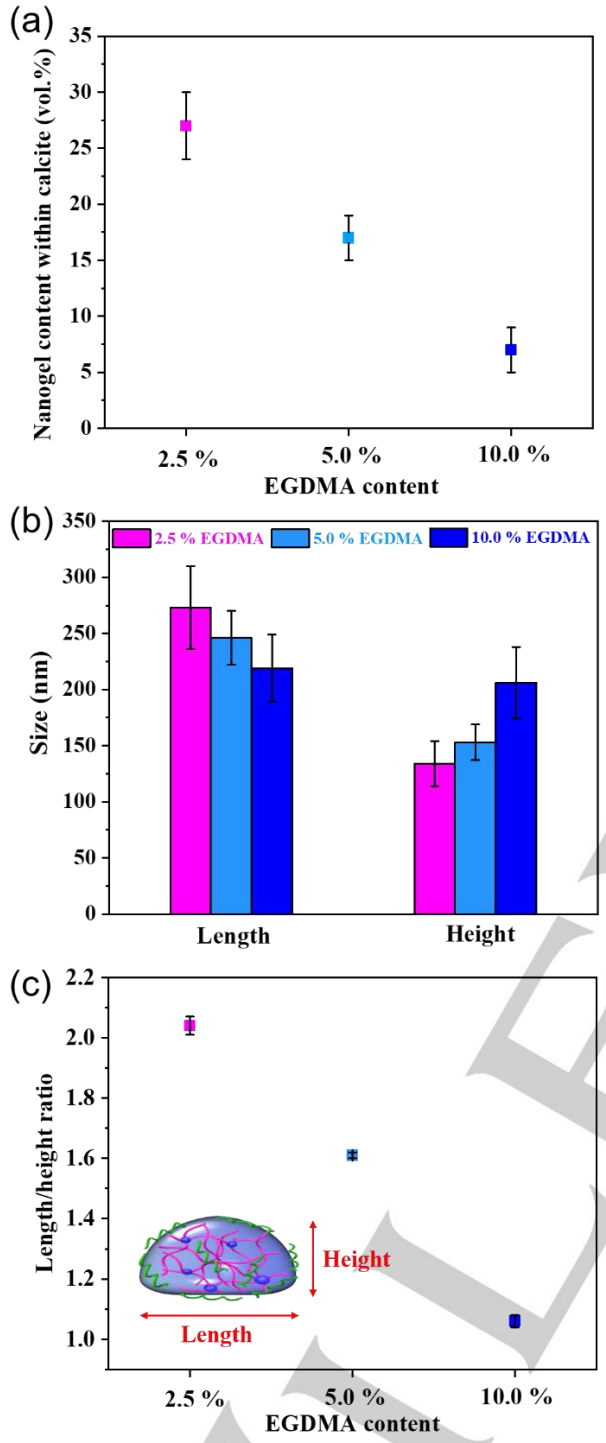

Figure 2. (a) Extent of nanogel occlusion within calcite crystals, as estimated by a stereological point counting method;[12] (b) mean lengths and heights for deformed nanogels observed after occlusion; (c) corresponding length/height ratios calculated for deformed nanogel particles containing 2.5%, 5.0% or 10.0% EGDMA.

Third, the cavity shape is strongly dependent on the EGDMA content of the nanogel particles. For nanogels containing 2.5% EGDMA, elongated cavities were observed (see **Figures 1e,f**). Given that SEM images of fractured calcite crystals only reflect the cross-sectional shape of the occluded nanogel particles, their actual morphology must be an elongated hemisphere. Increasing the EGDMA content to 5.0% led to a pseudo-hemispherical morphology (**Figures 1h,i**). In contrast, only spherical cavities were observed for nanogels containing 10.0% EGDMA (**Figures 1k,l**). This is because such highly cross-linked particles are much more resistant to deformation. Similar observations were made for occlusion experiments conducted using nanogels comprising 20.0% EGDMA (see **Figure S9**). Indeed, there are many literature examples of 'hard' polymeric nanoparticles or polymer-modified inorganic nanoparticles that retain their original spherical morphology after occlusion within calcite.[13]

For the EGDMA cross-linked nanogel particles, the mean length and height of the cavities were calculated to determine the length/height aspect ratio (**Figures 2b, 2c**). The latter parameter indicates the degree of deformation of the nanogel particles during their occlusion. Nanogels containing 2.5% EGDMA exhibit a length/height ratio of approximately 2.0, whereas those containing 5.0% or 10% EGDMA have length/height ratios of ≈ 1.6 or unity, respectively (see **Figure 2c**).

Finally, the most striking feature is that the deformed cavities are oriented in the same direction (see **Figures 1e, h**). Moreover, careful examination of the whole cross-section of a nanogel@calcite composite crystal revealed that this orientation is parallel to each (104) face of the host calcite crystals (see **Figure S10**). This suggests that there is a specific interaction between the nanogel particles and the growing calcite crystals, through which the nanogel particles always deform in the same direction and hence give rise to the observed orientation. Nanoparticle deformation during occlusion has been previously reported. For example, copolymer micelles became ellipsoidal during their engulfment within calcite and oil droplets also lose their initial spherical morphology under such conditions.[5a, 14] However, to the best of our knowledge, *local alignment* of deformed nanogel particles within calcite crystals has not yet been reported.

***In situ* AFM studies during nanogel particle occlusion.** *In situ* AFM studies were undertaken to gain further insights into the underlying mechanism for the morphological deformation and preferential orientation of the nanogel particles that occurs during their occlusion within calcite crystals (**Figure 3**). This technique involves using a macroscopic calcite crystal of geological origin and enables the entire occlusion process to be monitored in real time for individual nanogel particles.[15] As shown in **Figure S11a**, the growing calcite hillocks on the [16]nln face exhibit a typical rhombohedral morphology in a supersaturated solution at σ = 1.196 ($\sigma = ln\frac{a(Ca^{2+})a(CO_3^{2-})}{K_{sp}}$, K_{sp} =$10^{-8.54}$, $a(Ca^{2+})$ and $a(CO_3^{2-})$ are the activities of the calcium ion and carbonate ion, respectively).[17] At this point, a supersaturated solution (σ = 0.274, pH 8.3) containing 0.001% w/w 2.5% EGDMA nanogel particles is introduced. These soft particles adsorb onto the surface of the geologic calcite crystal and lateral deformation occurs (**Figure S11b**) prior to their occlusion, as indicated by a significant reduction in their height (see **Figure 3g**). Such deformation maximizes the contact area between the nanogel particles and the growing calcite surface, thus facilitating occlusion. Indeed, this explains why the nanogel particles with the lowest EGDMA content exhibit the highest extent of occlusion (**Figure 2a**). To initiate occlusion, a supersaturated $CaCO_3$ solution (σ = 1.196) was passed over the calcite crystal and the adsorbed nanogel

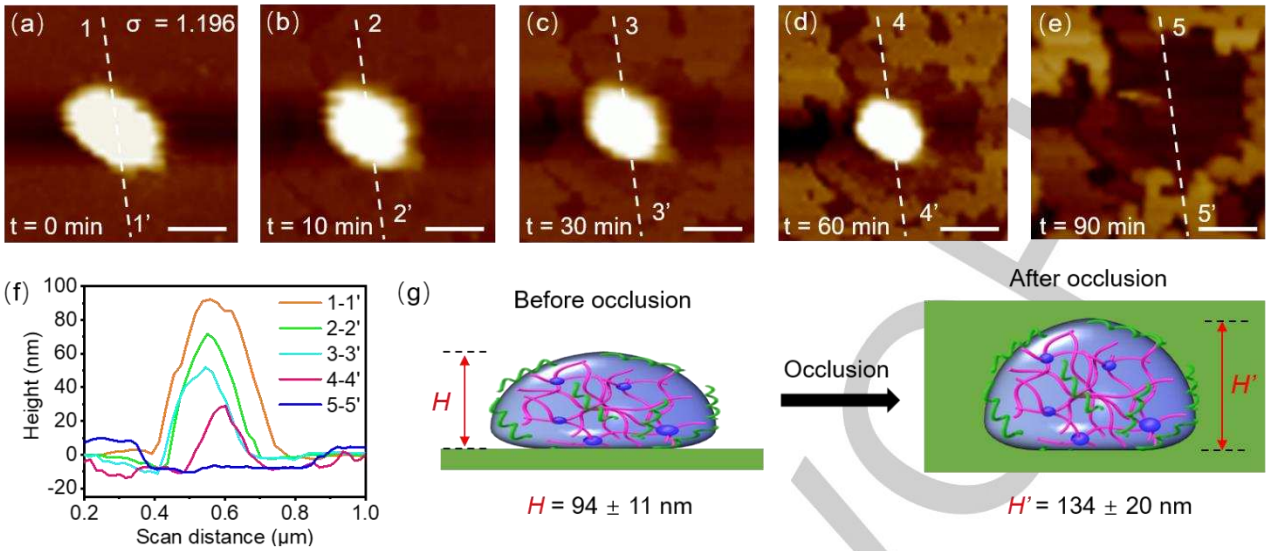

Figure 3. *In situ* monitoring of the occlusion of nanogel particles containing 2.5% EGDMA within a growing geological calcite crystal. (a-e) AFM images recorded for a representative nanogel particle at various time intervals (supersaturation (σ) = 1.196, pH 8.3). (f) Height profiles for this nanogel particle measured along the dashed lines shown in (a-e). These height profiles reflect the gradual engulfment of this nanogel particle within the growing calcite lattice. (g) Schematic cartoon showing the change in height of nanogel particle before (*H*) and after occlusion (*H'*). Scale bars in (a-e) equal 250 nm.

particles were gradually engulfed by the growing calcite (**Figures 3a-e**). This was accompanied by a reduction in height for each adsorbed nanogel particle (**Figure 3f**). Interestingly, the AFM height of the adsorbed 2.5% EDGMA nanogel particles prior to occlusion was determined to be 94 ± 11 nm, whereas the height of the final hemispherical cavity was estimated to be 134 ± 20 nm by SEM (see **Figure 3g**). This indicates that the adsorbed nanogel particles undergo vertical deformation during occlusion. This is physically reasonable because the guest nanoparticles experience a lateral compressive force exerted by the advancing crystal steps.[14a]

Mechanism of deformation and orientation of the nanogel particles within calcite. Based on the above observations, the occlusion of lightly cross-linked (2.5% EGDMA) nanogel particles within calcite involves three steps. First, nanogel particles adsorb onto the growing (104) face of calcite, followed by lateral deformation to produce a pseudo-hemispherical morphology. Second, the nanogel particles undergo vertical deformation during occlusion owing to compressive forces exerted by the growing steps, which leads to an increase in height. Finally, each nanogel particle becomes fully engulfed by the advancing crystal steps. This mechanism is summarized in **Figure 4**, which depicts the occlusion of a single nanogel particle on the (104) face of calcite for the sake of clarity. It is emphasized that rhombohedral calcite possesses six (104) faces.[18] Therefore, nanogel particles adsorb onto each of these faces concurrently during occlusion and the observed deformation is parallel to each face. Indeed, this was confirmed by imaging a large cross-sectional area of a fractured nanogel@calcite crystal (see **Figure S10**).

In prior studies, occlusion has been promoted by selecting an appropriate steric stabilizer.[19] Indeed, the extent of nanoparticle occlusion has been demonstrated to depend on the chemical nature of such steric stabilizer chains,[20] as well as their surface density,[21] chain length[13a] and charge density.[9] In contrast, the phosphonate functional groups that promote strong binding to calcite in the present study are primarily located within the nanogel cores. Moreover, close inspection of the inner cavities reveals many small protruding nanocrystals (**Figure 1l**), which suggests that the calcite partially penetrates the nanogel particles. This is not unexpected given that the nanogel particles are both highly swollen and deformable. Indeed, Li and coworkers reported that calcite crystals can readily penetrate within agarose gel networks.[22]

The lightly cross-linked nanogel particles used herein resemble certain globular proteins: both are spherical in shape, covalently stabilized and deformable.[23] Moreover, the deformability of the nanogel particles can be readily tuned by systematic variation of their EGDMA cross-linker content. In this sense, they provide an interesting model system for understanding the role played by proteins in biomineralization mechanisms, for which the

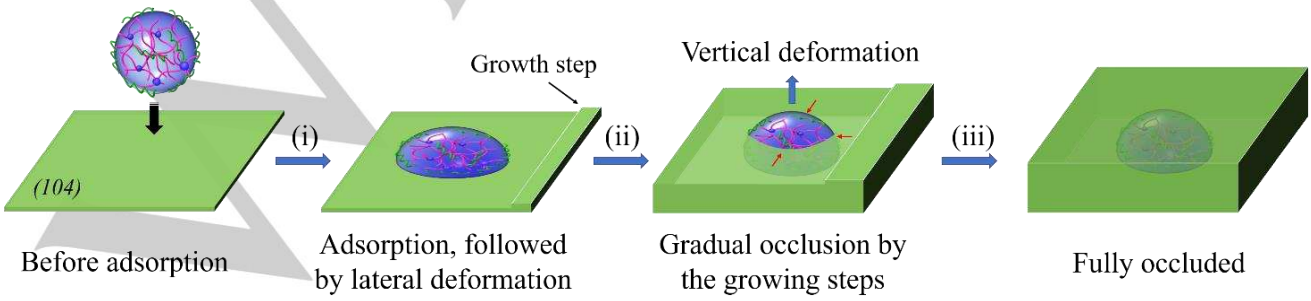

Figure 4. Schematic illustration of the deformation mechanism of the nanogel particles during the formation of nanogel@calcite composite crystals.

organic-mineral interaction is likely to be crucial.[24] To date, biomineralization research has mainly focused on how the organic component directs nucleation, crystal growth, crystal morphology and orientation.[25] It is widely recognized that the self-assembly of biopolymers or proteins to form ordered structures is essential for the subsequent spatially-controlled deposition of the mineral phase, and ultimately the formation of mechanically robust structures such as shells, bones and teeth.[26] However, whether mineralization influences the size, morphology and orientation of the organic phase has rarely been studied. In this context, the present study provides several new concepts. First, calcite mineralization certainly influences the nanogel morphology and the extent of this change is determined by the degree of nanogel deformability. More importantly, the resulting anisotropic nanogel particles are oriented normal to the growing (104) face of calcite.

It is well-established that nanoparticle occlusion within inorganic crystals offers an attractive and efficient synthetic route to functional hybrid materials.[14b, 27] However, the present study is the first to demonstrate that this strategy can be utilized to produce organic-inorganic nanocomposites possessing an oriented internal structure. Thus, it not only provides a unique model for understanding the intimate interaction between guest nanoparticles and host crystals but also opens up new opportunities for the rational design of novel nanocomposite materials with hierarchical complexity.

Conclusion

A series of nanogels of varying softness has been synthesized and employed for the mineralization of calcite single crystals. Highly crosslinked nanogels remain spherical after occlusion whereas lightly cross-linked nanogels experience significant deformation during their incorporation within the host crystal. Importantly, we demonstrate that additive@calcite artificial biominerals comprising oriented anisotropic nanoparticles can be prepared via a simple occlusion strategy. *In situ* AFM studies revealed the underlying mechanism for the formation of such ordered nanocomposite crystals, which provides useful insights regarding the mutual interaction between the organic and mineral phases that most likely occur during biomineralization. This study indicates that the rational design of highly-ordered multi-scale nanocomposite materials should be feasible via nanoparticle occlusion.

Acknowledgements

The authors thank Uni-Chemical Co., Ltd. (Nara, Japan) for donating PEM monomer. We gratefully acknowledge financial support from the National Natural Science Foundation of China (22101100), Basic and Applied Basic Research Project of Guangzhou (202201010237) and the Fundamental Research Funds for the Central Universities (21621032). S.P.A. thanks EPSRC for a four-year *Established Career* Particle Technology Fellowship (EP/R003009).

Keywords: nanogels • organic/inorganic nanocomposite crystals • biomineralization • nanoparticle occlusion • orientation

[1] a) S. Mann, *Biomineralization: principles and concepts in bioinorganic materials chemistry*, Oxford University Press, Oxford, **2001**; b) S. Mann, *Nature* **1988**, *332*, 119-124; c) H. A. Lowenstam, S. Weiner, *On biomineralization*, Oxford University Press on Demand, **1989**; d) A. Veis, *Science* **2005**, *307*, 1419-1420; e) F. C. Meldrum, H. Cölfen, *Chem. Rev.* **2008**, *108*, 4332-4432; f) R. A. Metzler, J. S. Evans, C. E. Killian, D. Zhou, T. H. Churchill, N. P. Appathurai, S. N. Coppersmith, P. U. P. A. Gilbert, *J. Am. Chem. Soc.* **2010**, *132*, 6329-6334.

[2] L. Addadi, D. Joester, F. Nudelman, S. Weiner, *Chem. Eur. J* **2006**, *12*, 980-987.

[3] L.-B. Mao, H.-L. Gao, H.-B. Yao, L. Liu, H. Cölfen, G. Liu, S.-M. Chen, S.-K. Li, Y.-X. Yan, Y.-Y. Liu, S.-H. Yu, *Science* **2016**, *354*, 107-110.

[4] a) Y. Ning, S. P. Armes, D. Li, *Macromol. Rapid Commun.* **2022**, *43*, 2100793; b) Y. Ning, S. P. Armes, *Acc. Chem. Res.* **2020**, *53*, 1176–1186; c) A. Lang, I. Polishchuk, G. Confalonieri, C. Dejoie, A. Maniv, D. Potashnikov, E. a. N. Caspi, B. Pokroy, *Adv. Mater.* **2022**, *34*, 2201652.

[5] a) Y.-Y. Kim, K. Ganesan, P. Yang, A. N. Kulak, S. Borukhin, S. Pechook, L. Ribeiro, R. Kröger, S. J. Eichhorn, S. P. Armes, *Nat. Mater.* **2011**, *10*, 890-896; b) Y. Ning, L. A. Fielding, J. Nutter, A. N. Kulak, F. C. Meldrum, S. P. Armes, *Angew. Chem. Int. Ed.* **2019**, *58*, 4302-4307; c) J. Ren, Y. Liu, H. Li, *J. Polym. Sci.* **2022**, *60*, 1151-1173.

[6] a) D. Athanasiadou, K. M. M. Carneiro, *Nat. Rev. Chem.* **2021**, *5*, 93-108; b) E. Pouget, E. Dujardin, A. Cavalier, A. Moreac, C. Valéry, V. Marchi-Artzner, T. Weiss, A. Renault, M. Paternostre, F. Artzner, *Nat. Mater.* **2007**, *6*, 434-439; c) H. Ehrlich, *Int. Geol. Rev.* **2010**, *52*, 661-699; d) D. Palin, R. W. Style, J. Zlopaša, J. J. Petrozzini, M. A. Pfeifer, H. M. Jonkers, E. R. Dufresne, L. A. Estroff, *J. Am. Chem. Soc.* **2021**, *143*, 3439-3447.

[7] H. Hanochi, T. L. Nguyen, S.-i. Yusa, Y. Nakamura, S. Fujii, *Langmuir* **2019**, *35*, 6993-7002.

[8] a) Y. Ning, L. Han, M. J. Derry, F. C. Meldrum, S. P. Armes, *J. Am. Chem. Soc.* **2019**, *141*, 2557-2567; b) J. P. Hindmarsh, P. Watkinson, *J. Dairy Sci.* **2017**, *100*, 6938-6948.

[9] M. Douverne, Y. Ning, A. Tatani, F. C. Meldrum, S. P. Armes, *Angew. Chem. Int. Ed.* **2019**, *58*, 8692-8697.

[10] F. A. Plamper, W. Richtering, *Acc. Chem. Res.* **2017**, *50*, 131-140.

[11] J. Ihli, P. Bots, A. Kulak, L. G. Benning, F. C. Meldrum, *Adv. Funct. Mater.* **2013**, *23*, 1965-1973.

[12] J. C. Russ, R. T. Dehoff, *Practical stereology*, Springer Science & Business Media, **2012**.

[13] a) Y. Ning, L. Han, M. Douverne, N. J. Penfold, M. J. Derry, F. C. Meldrum, S. P. Armes, *J. Am. Chem. Soc.* **2019**, *141*, 2481-2489; b) Y. Dong, Z. Liu, Y. Ning, S. P. Armes, D. Li, *Chem. Mater.* **2022**, *34*, 3357-3364; c) Y.-Y. Kim, R. Darkins, A. Broad, A. N. Kulak, M. A. Holden, O. Nahi, S. P. Armes, C. C. Tang, R. F. Thompson, F. Marin, *Nat. Commun.* **2019**, *10*, 5682; d) O. Nahi, A. N. Kulak, T. Kress, Y.-Y. Kim, O. G. Grendal, M. J. Duer, O. J. Cayre, F. C. Meldrum, *Chem. Sci.* **2021**, *12*, 9839-9850.

[14] a) K. R. Cho, Y.-Y. Kim, P. Yang, W. Cai, H. Pan, A. N. Kulak, J. L. Lau, P. Kulshreshtha, S. P. Armes, F. C. Meldrum, J. J. De Yoreo, *Nat. Commun.* **2016**, *7*, 10187; b) Y. Ning, F. C. Meldrum, S. P. Armes, *Chem. Sci.* **2019**, *10*, 8964-8972.

[15] a) J. Chi, W. Zhang, C. V. Putnis, L. Wang, *Cryst. Growth & Des.* **2021**, *21*, 2398-2404; b) J. Chi, W. Zhang, L. Wang, C. V. Putnis, *Environ. Sci. Technol.* **2019**, *53*, 8097-8104; c) C. T. Hendley IV, L. A. Fielding, E. R. Jones, A. J. Ryan, S. P. Armes, L. A. Estroff, *J. Am. Chem. Soc.* **2018**, *140*, 7936-7945; d) M. K. Choudhary, R. Jain, J. D. Rimer, *PNAS* **2020**, *117*, 28632-28639.

[16] **!!! INVALID CITATION !!! {}**.

[17] H. H. Teng, P. M. Dove, C. A. Orme, J. J. De Yoreo, *Science* **1998**, *282*, 724-727.

[18] a) J. W. Morse, R. S. Arvidson, A. Lüttge, *Chem. Rev.* **2007**, *107*, 342-381; b) S. Hashmi, H. Wickman, D. Weitz, *Phys. Rev. E* **2005**, *72*, 041605.

[19] a) Y. Ning, D. J. Whitaker, C. J. Mable, M. J. Derry, N. J. Penfold, A. N. Kulak, D. C. Green, F. C. Meldrum, S. P. Armes, *Chem. Sci.* **2018**, *9*, 8396-8401; b) R. Muñoz‐Espí, Y. Qi, I. Lieberwirth, C. M. Gómez, G. Wegner, *Chem. Eur. J* **2006**, *12*, 118-129.

[20] a) Y. Ning, L. A. Fielding, K. E. Doncom, N. J. Penfold, A. N. Kulak, H. Matsuoka, S. P. Armes, *ACS Macro Lett.* **2016**, *5*, 311-315; b) Z. Liu, B. Xiong, Y. Dong, Y. Ning, D. Li, *Inorg. Chem.* **2022**, *61*, 16203-16210; c) O. Nahi, A. Broad, A. N. Kulak, H. M. Freeman, S. Zhang, T. D. Turner, L. Roach, R. Darkins, I. J. Ford, F. C. Meldrum, *Chem. Mater.* **2022**, *34*, 4910–4923.

[21] Y. Ning, L. A. Fielding, L. P. Ratcliffe, Y.-W. Wang, F. C. Meldrum, S. P. Armes, *J. Am. Chem. Soc.* **2016**, *138*, 11734-11742.

[22] a) H. Li, H. L. Xin, D. A. Muller, L. A. Estroff, *Science* **2009**, *326*, 1244-1247; b) Y. Liu, W. Yuan, Y. Shi, X. Chen, Y. Wang, H. Chen, H. Li, *Angew. Chem. Int. Ed.* **2014**, *53*, 4127-4131; c) Y. Liu, H. Zang, L. Wang, W. Fu, W. Yuan, J. Wu, X. Jin, J. Han, C. Wu, Y. Wang, *Chem. Mater.* **2016**, *28*, 7537-7543.

[23] a) N. Nussbaum, J. Bergfreund, J. Vialetto, L. Isa, P. Fischer, *Colloids Surf. B: Biointerfaces* **2022**, *217*, 112595; b) S. Matsui, T. Kureha, S. Hiroshige, M. Shibata, T. Uchihashi, D. Suzuki, *Angew. Chem. Int. Ed.* **2017**, *56*, 12146-12149; c) M. Rey, M. A. Fernandez-Rodriguez, M. Karg, L. Isa, N. Vogel, *Acc. Chem. Res.* **2020**, *53*, 414-424; d) L. Hoppe Alvarez, A. A. Rudov, R. A. Gumerov, P. Lenssen, U. Simon, I. I. Potemkin, D. Wöll, *Phys. Chem. Chem. Phys.* **2021**, *23*, 4927-4934; e) L. Hoppe Alvarez, S. Eisold, R. A. Gumerov, M. Strauch, A. A. Rudov, P. Lenssen, D. Merhof, I. I. Potemkin, U. Simon, D. Wöll, *Nano Lett.* **2019**, *19*, 8862-8867.

[24] a) O. Branson, E. A. Bonnin, D. E. Perea, H. J. Spero, Z. Zhu, M. Winters, B. Hönisch, A. D. Russell, J. S. Fehrenbacher, A. C. Gagnon, *PNAS* **2016**, *113*, 12934-12939; b) P. Gilbert, M. Abrecht, B. H. Frazer, Geochemistry, *Rev. Mineral. Geochem.* **2005**, *59*, 157-185; c) S. Mann, D. D. Archibald, J. M. Didymus, T. Douglas, B. R. Heywood, F. C. Meldrum, N. J. Reeves, *Science* **1993**, *261*, 1286-1292; d) A.-W. Xu, Y. Ma, H. Cölfen, *J. Mater. Chem.* **2007**, *17*, 415-449.

[25] L.-B. Mao, Y.-F. Meng, X.-S. Meng, B. Yang, Y.-L. Yang, Y.-J. Lu, Z.-Y. Yang, L.-M. Shang, S.-H. Yu, *J. Am. Chem. Soc.* **2022**, *144*, 18175-18194.

[26] a) C. Du, G. Falini, S. Fermani, C. Abbott, J. Moradian-Oldak, *Science* **2005**, *307*, 1450-1454; b) F. Nudelman, N. A. Sommerdijk, *Angew. Chem. Int. Ed.* **2012**, *51*, 6582-6596.

[27] a) O. Nahi, A. Broad, A. N. Kulak, H. M. Freeman, S. Zhang, T. D. Turner, L. Roach, R. Darkins, I. J. Ford, F. C. Meldrum, *Chem. Mater.* **2022**, *34*, 4910-4923; b) B. Marzec, J. Walker, Y. Jhons, F. C. Meldrum, M. Shaver, F. Nudelman, *Faraday Discuss.* **2022**, *235*, 536-550; c) J. Ren, M. Niu, X. Guo, Y. Liu, X. Yang, M. Chen, X. Hao, Y. Zhu, H. Chen, H. Li, *J. Am. Chem. Soc.* **2020**, *142*, 1630-1635; d) G. Lu, S. Li, Z. Guo, O. K. Farha, B. G. Hauser, X. Qi, Y. Wang, X. Wang, S. Han, X. Liu, *Nat. Chem.* **2012**, *4*, 310-316; e) M. Zhang, H. Ping, W. Fang, F. Wan, H. Xie, Z. Zou, Z. Fu, *J. Mater. Chem. B* **2020**, *8*, 9269-9276; f) Y. Ning, Y. Han, L. Han, M. J. Derry, S. P. Armes, *Angew. Chem. Int. Ed.* **2020**, *59*, 17966-17973; g) J. D. Xiao, Q. Shang, Y. Xiong, Q. Zhang, Y. Luo, S. H. Yu, H. L. Jiang, *Angew. Chem. Int. Ed.* **2016**, *55*, 9389-9393.

Entry for the Table of Contents

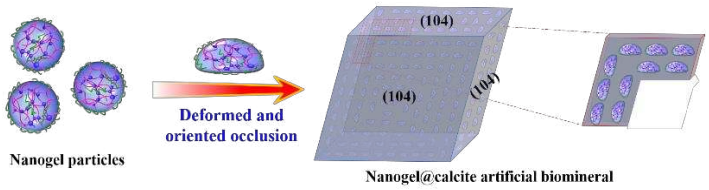

Controlled deformation of soft nanogel particles during their occlusion within calcite crystals enables the generation of artificial biominerals with oriented internal structure. This model system provides new mechanistic insights regarding the formation of oriented structures during biomineralization and indicates that the rational design of multi-scale nanocomposite materials should be feasible via nanoparticle occlusion.

Prof. Ning's Twitter usernames: @YinNing7

Prof. Armes' Twitter usernames: @ArmesGroup